Journal of Materials Chemistry A

RSC Publishing

PAPER

View Article Online
View Journal | View Issue



Cite this: J. Mater. Chem. A, 2013, 1, 15423

# Synthesis and characterization of graphene hollow spheres for application in supercapacitors†

Qingguo Shao,[ab] Jie Tang,*[ab] Yuexian Lin,[ab] Feifei Zhang,[ab] Jinshi Yuan,[a] Han Zhang,[a] Norio Shinya[a] and Lu-Chang Qin[c]

Received 18th July 2013
Accepted 12th October 2013

DOI: 10.1039/c3ta12789c

www.rsc.org/MaterialsA

We have successfully assembled graphene nanosheets into spherical shells using polystyrene spheres as templates. Compared with stacked planar graphene, the as-prepared graphene spherical shells have more free space in between the spheres, which results in a larger accessible surface area for adsorption of electrolyte ions in supercapacitors. Electrochemical tests show that the graphene hollow spheres exhibit a high specific capacitance of 273 F $g^{-1}$ and excellent electrochemical stability.

## Introduction

Due to its exceptional physical, chemical, and mechanical properties, graphene, a one-atom-thick two-dimensional carbon material, has become a promising candidate for a broad range of applications. Graphene offers large specific surface area, high conductivity, excellent mechanical flexibility, and outstanding chemical stability. These characteristics make graphene an attractive electrode material for supercapacitors.[1–5] Stoller *et al.* first reported that chemically modified graphene can deliver a specific capacitance of 135 F $g^{-1}$ and 99 F $g^{-1}$ in aqueous and organic electrolytes, respectively.[6] However, the graphene sheets tend to restack due to the strong π–π interactions and van der Waals forces between them, which cause a significant decrease in the electrochemically active surface area and the inter-graphene channels accessible to electrolyte, leading to lower specific capacitance.[7] Therefore, a key issue in graphene supercapacitors is to reduce the agglomeration of graphene sheets during material processing in assembling them into macroscopic structures for device applications. Until now, several useful strategies have emerged to prevent the restacking of graphene sheets, including (i) tailoring the solvent–graphene interactions, (ii) utilizing dispersing agents, (iii) crumpling the graphene sheets, and (iv) compositing graphene with metal oxides.[8–11] In addition to these the idea of adding a spacer between graphene sheets seems to be most effective and promising. For example, carbon black and small graphite particles have been used as the spacer.[7,12] In our previous work we have also explored the use of single-walled carbon nanotubes as spacers to reduce agglomeration of graphene sheets and found that the electrochemical properties of the composite graphene electrodes were indeed much improved.[13]

In recent years, much attention has been paid to assemble graphene nanosheets into various tailored macroscopic graphene structures, such as porous films, flowers, networks, and hydrogels, to improve their electrochemical performance.[14–17] More recently, graphene capsules have been synthesized by W/O emulsion and capillary molding and the as-prepared graphene capsules showed attractive characteristics for oil absorption.[18–20]

In the present study, we have successfully assembled graphene nanosheets into hollow spherical shells and tested them as electrode materials for supercapacitors. Compared with planar stacked graphene sheets, the hollow spherical graphene shells can provide more free space between the spheres and therefore reduce effective restacking of graphene sheets. A more accessible surface area can also be produced for ion adsorption. Electrochemical characterization shows that the graphene hollow spheres exhibit an impressive specific capacitance of 273 F $g^{-1}$ at a low current density of 0.5 A $g^{-1}$ and 197 F $g^{-1}$ at a high current density of 10 A $g^{-1}$, respectively. Moreover, when they were charged and discharged repeatedly at a high current density of 10 A $g^{-1}$, they retained 95% of their initial capacitance even after 5000 cycles. These findings indicate that the graphene hollow spheres are promising as electrode materials for supercapacitors.

## Experimental

### Synthesis of positively charged PS spheres

The positively charged polystyrene (PS) spheres were prepared by dispersive polymerization.[21] In this work, 20 mL of styrene monomers and 0.5 g of PVP were first added to 100 mL of deionized water in a 250 mL flask in a water bath. After stirring at 400 rpm for 30 minutes, 0.2 g of AIBA dissolved in 20 mL of

[a]National Institute for Materials Science, 1-2-1 Sengen, Tsukuba 305-0047, Japan. E-mail: tang.jie@nims.go.jp

[b]Doctoral Program in Materials Science and Engineering, University of Tsukuba, 1-1-1 Tennodai, Tsukuba 305-8577, Japan. E-mail: tang.jie@nims.go.jp

[c]Department of Physics and Astronomy, University of North Carolina at Chapel Hill, Chapel Hill, NC 27599-3255, USA. E-mail: lcqin@unc.edu

† Electronic supplementary information (ESI) available. See DOI: 10.1039/c3ta12789c

deionized water was added. The mixture was deoxygenated by bubbling nitrogen gas for 30 min, and then it was kept at 70 °C for 24 hours before cooling to room temperature. After the reaction completed, the product was centrifuged in methanol and deionized water and dried in an oven overnight.

### Synthesis of PS@graphene core–shell spheres

Graphene oxide was synthesized from natural graphite flakes by a modified Hummers method.[22] Specifically, 30 mg of graphene oxide powders and 70 mg of PS spheres were dispersed in 50 mL of deionized water separately aided by sonication. The two solutions were then mixed together and sonicated for another hour. The mixture was heated to 100 °C and 0.5 mL of hydrazine hydrate was added into the mixture. The reaction was kept going at 98 °C for 6 more hours. The product was harvested by centrifugation and washed with deionized water before drying in an oven overnight.

### Synthesis of graphene hollow spheres

The above prepared PS@graphene core–shell spheres were placed at the center of a tube furnace and were heated to 420 °C with a heating rate of 5 °C per minute and maintained at this temperature in air for 2 hours.

### Structural characterization

The material morphology and structure were examined with a field-emission scanning electron microscope (FE-SEM, JSM-6500, JEOL, Japan) and transmission electron microscope (TEM, JEM-2100, JEOL, Japan). Powder X-ray diffraction (XRD) patterns were recorded with a Rigaku RINT 2500. Raman spectra were obtained with a RAMAN-11 (Nanophoton) with a 532 nm laser source. Thermogravimetric (TG) analysis was performed on an SDTA851e Analyzer at a heating rate of 10 °C $min^{-1}$ in air. The specific surface area and pore size distribution were measured with an AUTOSORB of Quantachrome Instruments.

### Electrochemical characterization

The electrochemical properties of graphene hollow spheres were investigated using a three-electrode test system.[23] The working electrode was fabricated by mixing the prepared powders with 10 wt% polytetrafluorene-ethylene (PTFE) binder. The mixture was pressed onto nickel foam to make electrodes. A platinum foil and a saturated Ag/AgCl electrode were used as the counter and the reference electrode, respectively. A 5 M KOH solution was used as the electrolyte. Cyclic voltammetry, galvanostatic charge–discharge, and electrochemical impedance spectroscopy were performed on an EC-lab electrochemical workstation. The specific capacitance of the electrode was obtained from the discharge process according to the following equation

$$C_g = \frac{I \times \Delta t}{m \times \Delta V}$$

where $I$ is the loaded current, $\Delta t$ is the discharge time, $\Delta V$ is the potential drop during discharge, and $m$ is the mass of active material in a single electrode.

## Results and discussion

Fig. 1 illustrates the preparation of the spherical graphene shells. The synthesis consists of two steps: (i) formation of PS@graphene core–shell spheres and (ii) removal of PS template spheres. Positively charged PS spheres were first prepared by a solution polymerization method using AIBA as an initiator. Then they were mixed with negatively charged graphene oxide nanosheets. At the beginning, due to the electrostatic attractions, graphene oxide sheets would wrap around the PS spheres to neutralize the positive charges. Then, other graphene oxide sheets would be adsorbed on the wrapped graphene shells because of the π–π interactions and the van der Waals forces. As a result, the PS spheres would act like "nucleation centers" to roll the graphene oxide sheets into spherical shells. After being reduced by hydrazine, the PS@graphene core–shell structure was produced. Finally, the PS template spheres were removed by heat treatment and graphene hollow spheres were obtained.

Fig. 2 shows SEM images of the as-prepared (A) PS spheres, (B) PS@graphene core–shell spheres, and (C) graphene hollow spheres. As can be observed in Fig. 2(A), the PS spheres are not only mono-dispersed with an average diameter of ~290 nm but also have smooth surfaces. Fig. 2(B) is a typical SEM image of the PS@graphene core–shell spheres. It can be clearly seen that the graphene nanosheets are uniformly coated on the surface of PS spheres, leading to a core–shell structure. In addition, it should be pointed out that the electrostatic attraction between the GO sheets and the PS spheres plays a key role in the formation of the core–shell structure. Fig. 2(C) shows the final graphene hollow spheres, after removing the PS template, and the spherical geometry was retained. The SEM image also indicates that the graphene layers were very thin.

The morphology and structure of the PS@graphene core–shell spheres and the graphene hollow spheres were also characterized by TEM. Fig. 3(A) and (B) display representative TEM images of PS@graphene core–shell spheres. In Fig. 3(A) we can find that the neighboring spheres are linked together by a thin sheet, which provides direct visual evidence for the presence of graphene nanosheets. Besides, the rough surface of one core–shell sphere shown in Fig. 3(B) confirms the graphene coating. Fig. 3(C) shows a TEM image at low magnification of the spherical graphene. Nearly all the graphene spheres show a

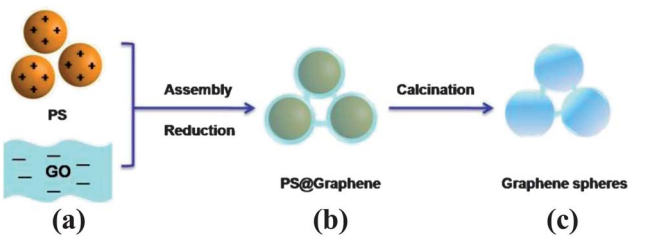


**Fig. 1** Illustration of the preparation process of graphene hollow spheres. (a) PS spheres and GO are mixed; (b) graphene shells are formed on the PS spheres; and (c) PS spheres are removed to obtain spherical graphene shells.

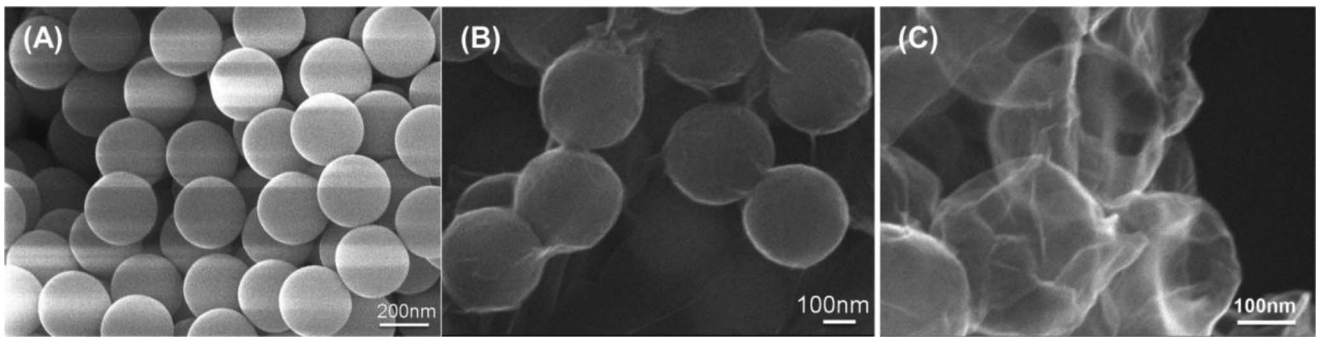


**Fig. 2** SEM images of as prepared structures: (A) PS spheres of uniform size, (B) PS@graphene core–shell spheres, and (C) graphene spherical shells after removal of the PS spheres in the core.

hollow structure. The enlarged TEM image (Fig. 3(D)) reveals that the diameter of the hollow spheres is about 300 nm and the shell thickness is about 8 nm.

Fig. 4 shows the XRD patterns of graphite (green), graphite oxide (blue), and graphene spheres (red). For pristine graphite the Bragg peak at $2\theta = 26.2^\circ$ is due to the (002) reflection with an interlayer spacing of 0.34 nm.[24] However, for graphite oxide this peak disappeared and a broader reflection peak appeared at $2\theta = 10.0^\circ$, corresponding to an interlayer spacing of 0.89 nm, which is attributed to the intercalation of oxygen functional groups. After having been reduced by hydrazine, the XRD pattern of graphene spheres shows a typical broad peak

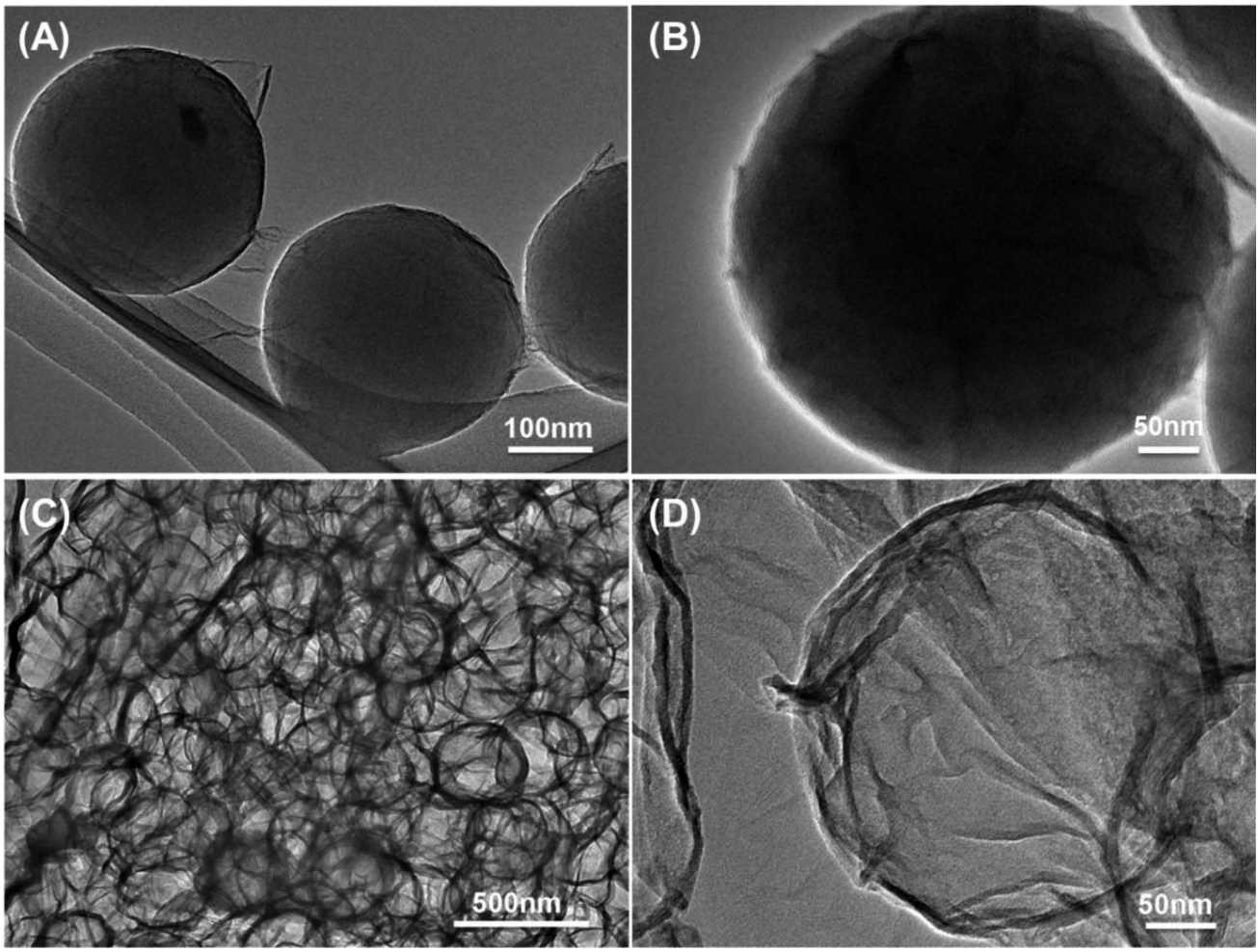


**Fig. 3** TEM images of (A and B) PS@graphene core–shell spheres and (C and D) graphene hollow spheres. After the graphene shells were formed, the neighboring spheres are often connected with graphene sheets.

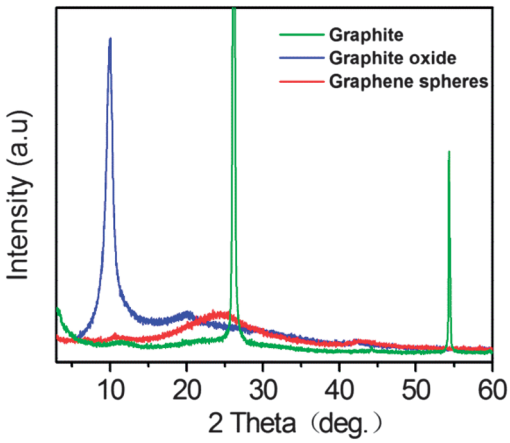


**Fig. 4** XRD pattern of graphite (green), graphite oxide (blue), and graphene hollow spheres (red).

at $2\theta = 24.1°$, corresponding to an interlayer spacing of 0.36 nm, which is a little larger than that of graphite. These results indicate that the graphene spheres were highly reduced, resulting in a new structure which is significantly different from the pristine graphite and graphite oxide.

The structural evolution of PS, PS@GO, PS@graphene, and graphene hollow spheres was also characterized by Raman spectroscopy as shown in Fig. 5. The Raman spectrum of PS spheres shows three weak characteristic peaks at 1180, 1450, and 1610 $cm^{-1}$, and these weak signals were attenuated or absorbed when the PS spheres were wrapped by graphene oxide or graphene. As for the Raman spectrum of PS@GO, PS@graphene and graphene hollow spheres, the two intense features are the D band at 1340 $cm^{-1}$ and the G band at 1590 $cm^{-1}$.

The D band is associated with disorder arising from structural defects, while the G band corresponds to the first-order scattering of the stretching vibrational mode $E_{2g}$ observed due to the $sp^2$ bonded carbon domains.[25] In general, the intensity ratio of D band to G band ($I_D/I_G$) indicates the degree of disorder. Compared with the spectrum of PS@GO, as shown in Fig. 5, $I_D/I_G$ increased in the spectrum of PS@graphene. This occurs because of the increased number of structural defects after reduction. The ratio of $I_D/I_G$ decreased a little from PS@graphene to graphene hollow spheres, which is attributed to the improved crystallinity of graphene by heat treatment.

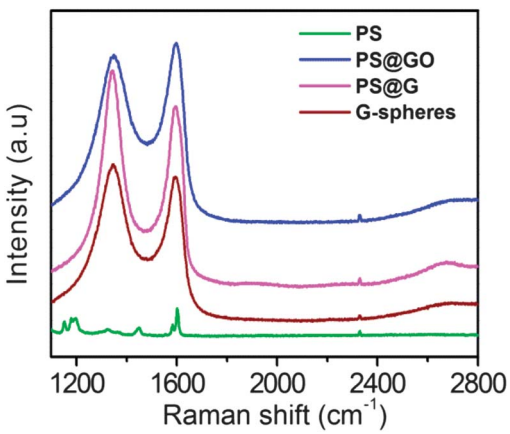


**Fig. 5** Raman spectra of as-prepared structures of PS (green), PG@GO (blue), PS@graphene core shell spheres (purple), and graphene hollow spheres (brown).

Fig. 6 shows the TG curves of PS spheres and PS@graphene core–shell spheres. As shown in Fig. 6(A), the PS spheres began to decompose at 300 °C and were burned completely at 410 °C. However, as expected, the PS@graphene core–shell spheres showed a two-step process in weight loss (Fig. 6(B)), corresponding to the decomposition of PS cores and graphene shells, respectively. The graphene shells began to decompose significantly at about 450 °C. Therefore, in the case of our heat treatment at a temperature of 420 °C, the PS spheres were removed while the graphene shells were retained. Besides, the TG measurement (ESI, Fig. S1†) of pure graphene under the same heating conditions (air; 30–420 °C, heating rate 5 °C $min^{-1}$; held at 420 °C for 2 hours) also confirmed that most of the graphene (78%) can be retained under these conditions.

The BET surface area of graphene hollow spheres was obtained from the nitrogen adsorption–desorption isotherms shown in Fig. 7. The isotherms (Fig. 7(A)) exhibited a mixed type-II and type-V characteristics, indicating the presence of microporosity, mesoporosity, and macroporosity. A specific surface area of about 440 $m^2\ g^{-1}$ for the as-prepared graphene hollow spheres was obtained by the BET measurement. The corresponding pore size distribution (Fig. 7(B)) exhibited an average pore diameter of 3.2 nm calculated by the DFT model, which is ascribed to the space between graphene spheres.

The obtained graphene hollow spheres were also investigated as electrode materials for supercapacitors. The electrochemical properties were tested using cyclic voltammetry (CV) and galvanostatic charge–discharge measurements within the potential window of −1 to −0.2 V in 5 M KOH aqueous solution. Fig. 8(A) shows the CV curves of graphene hollow spheres at scan rates of 10–50 mV $s^{-1}$. The curves are approximately rectangular in shape, indicating an excellent capacitive behaviour. Accordingly, the galvanostatic charge–discharge curves at various current densities as shown in Fig. 8(B) are symmetric triangles without obvious potential drop (IR drop), confirming the characteristic electric double-layer capacitance. The calculated specific capacitance at different current densities is displayed in Fig. 8(C). Specific capacitances of 273, 244, 224, and 208 F $g^{-1}$ were obtained for the graphene hollow spheres at

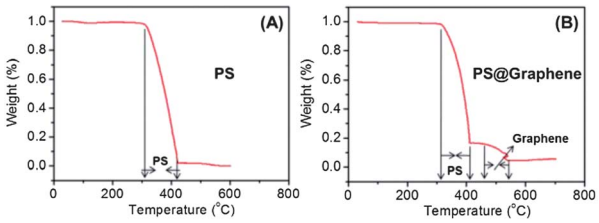


**Fig. 6** TG curves of (A) PS spheres and (B) PS@graphene core–shell spheres. Gravimetric loss of graphene starts at 450 °C.

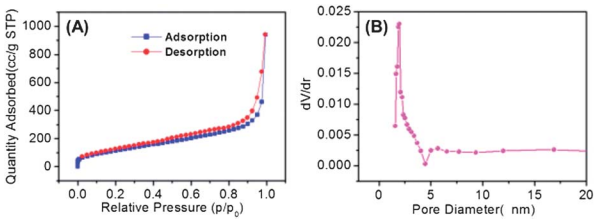


**Fig. 7** Nitrogen sorption isotherms of (A) graphene hollow spheres and (B) corresponding pore size distribution. The average diameter of pores is 3.2 nm.

current densities of 0.5, 1.0, 2.0, and 5.0 A $g^{-1}$, respectively. Even charged and discharged at high current densities of 10 and 20 A $g^{-1}$, the graphene hollow spheres retained a high specific capacitance of 197 and 183 F $g^{-1}$, respectively, highlighting excellent rate capability. In order to investigate the durability of the graphene hollow spheres, a repetitive charge–discharge cycling test was carried out at a high current density of 10 A $g^{-1}$ over 5000 cycles. As shown in Fig. 8(D), the graphene hollow spheres retained 95% of their initial capacitance even after 5000 cycles. The excellent cyclability is attributed to the fewer oxygen-containing functional groups (ESI, Fig. S2†) in the material which is largely responsible for faradaic pseudocapacitance. The cyclability is much improved in comparison with many of the previously reported pure graphene structures including thermally exfoliated graphene, nitrogen-modified graphene, vacuum-promoted exfoliated graphene, and even better than many of the graphene composites, such as CNT/graphene, $MnO_2$/graphene, and $Mn_3O_4$/graphene electrodes.[26–31]

We attribute the outstanding capacitive behaviour of graphene hollow spheres to their unique spherical structure (the graphene hollow spheres can maintain their structure after being processed to fabricate supercapacitor electrodes (ESI, Fig. S3†)). Compared with planar graphene sheets, the graphene hollow spheres are advantageous due to their unique features in structure: (1) spherical graphene can significantly reduce large stacks of graphene sheets and makes more accessible surface area available for electrolyte ion adsorption; (2) there are more free spaces between graphene spheres, which can make the graphene shells fully wetted by electrolyte; and (3) the graphene spheres are interconnected, which would in turn improve electrical conduction of the electrode.

We also suggest that the graphene spheres reported in this work would find potential applications in other fields such as lithium ion batteries, electrochemical sensors, and oil absorption.

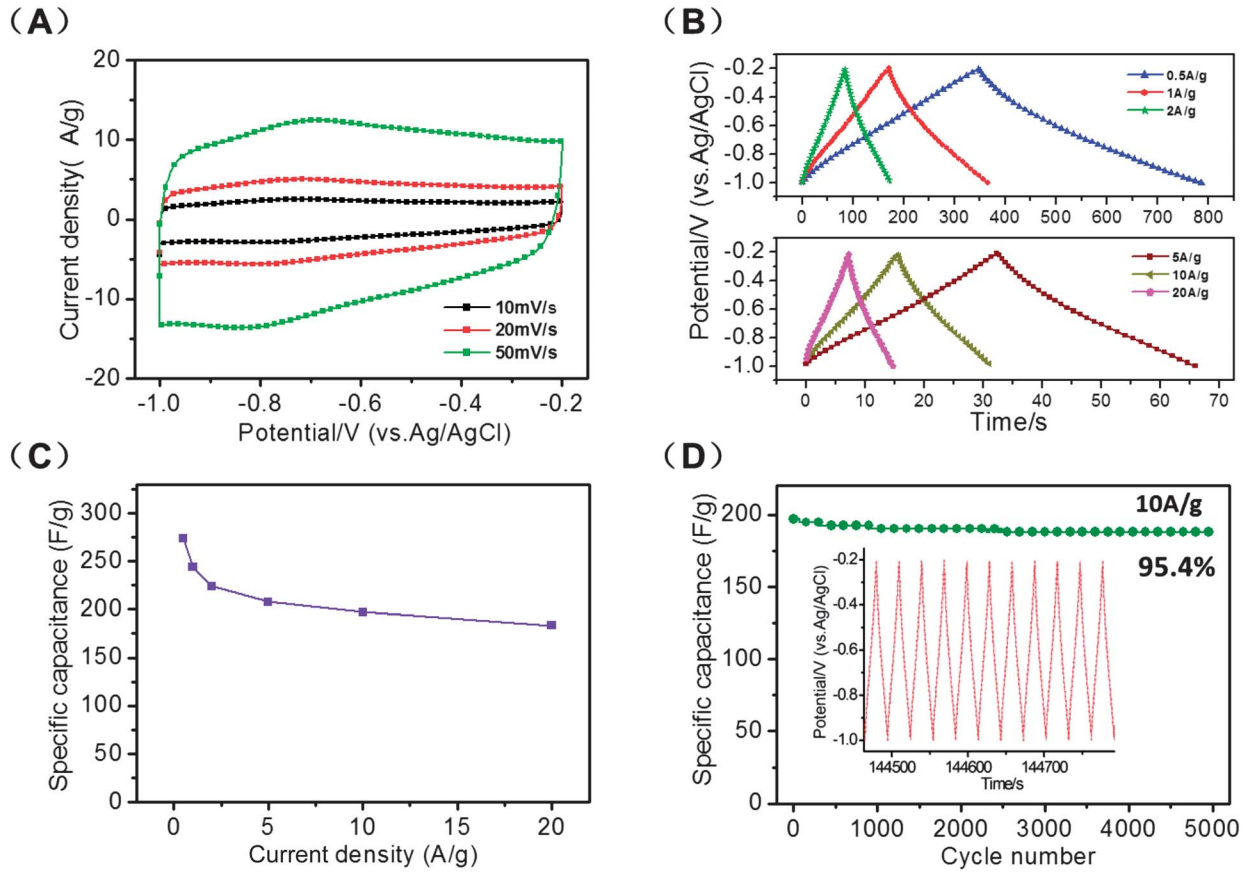


**Fig. 8** Electrochemical characterization of as-prepared graphene hollow spheres. (A) Cyclic voltammograms at various scan rates; (B) galvanostatic charge–discharge curves; (C) corresponding specific capacitance at various current densities, and (D) cyclability at a high current density of 10 A $g^{-1}$ (inset is a portion of the charge–discharge curve after 40 hours).

## Conclusions

We have successfully fabricated spherical graphene shells using polystyrene spheres as templates. The as-prepared graphene hollow spheres were studied as electrode materials for supercapacitors. Compared with stacked planar graphene, the graphene hollow spheres offer more free space between spheres, leading to a larger accessible surface area for ion adsorption. Electrochemical tests showed that the graphene hollow spheres exhibited a high specific capacitance of 273 F $g^{-1}$ at a current density of 0.5 A $g^{-1}$ and 197 F $g^{-1}$ at a higher current density of 10 A $g^{-1}$. After charge–discharge of 5000 cycles at a high current density of 10 A $g^{-1}$, the graphene hollow spheres retained 95% of their initial capacitance. These results demonstrate that the graphene hollow spheres are a promising structure for supercapacitor applications.

## Acknowledgements

This work was financially supported by the JST ALCA Program (no. 22310074), JSPS Grants-in-Aid for Scientific Research (no. 22310074), and the Nanotechnology Network Project of MEXT, Japan.

## Notes and references

1 Y. W. Zhu, S. Murali, W. W. Cai, X. Li, J. Suk, J. R. Potts and R. S. Ruoff, *Adv. Mater.*, 2010, **22**, 3906–3924.
2 K. S. Novoselov, A. K. Geim, S. V. Morozov, D. Jiang, Y. Zhang, S. V. Dubonos, I. V. Grigorieva and A. A. Firsov, *Science*, 2004, **306**, 666–669.
3 J. J. Wang, M. Y. Zhu, R. A. Outlaw, X. Zhao, D. M. Manos and B. C. Holloway, *Carbon*, 2004, **42**, 2867–2872.
4 S. William, J. Hummers and E. Richard, *J. Am. Chem. Soc.*, 1958, **80**, 1339.
5 D. C. Marcano, D. V. Kosynkin, J. M. Berlin, A. Sinitskii, Z. Sun, A. Slesarev, L. B. Alemany, W. Lu and M. James, *ACS Nano*, 2010, **4**, 4806–4814.
6 M. D. Stoller, S. J. Park, Y. W. Zhu, J. H. An and R. S. Ruoff, *Nano Lett.*, 2008, **8**, 3498–3502.
7 J. Yan, T. Wei, B. Shao, F. Q. Ma, Z. J. Fan, M. L. Zhang, C. Zheng, Y. C. Shang, W. Z. Qian and F. Wei, *Carbon*, 2010, **48**, 1731–1737.
8 X. Yang, J. Zhu, L. Liu and D. Li, *Adv. Mater.*, 2011, **23**, 2833–2838.
9 J. Luo, S. H. D. Jang, T. Sun, L. Xiao, H. Zhen, A. Katsooulidis, M. Kanatzidis, J. Gibson and J. Huang, *ACS Nano*, 2011, **5**, 8943–8949.
10 Z. Wen, X. Wang, S. Mao, Z. Bo, H. Kim, S. Cui, C. Lu, X. Feng and J. Chen, *Adv. Mater.*, 2012, **24**, 5610–5616.
11 X. Feng, Z. Yan, N. Cheng, Y. Zhang, Y. Ma, X. Liu, N. Cheng, Q. Fan, L. Wang and W. Huang, *J. Mater. Chem. A*, 2013, **1**, 12818–12825.
12 X. Du, H. Song and X. Chen, *J. Mater. Chem.*, 2012, **22**, 13091–13096.
13 Q. Cheng, J. Tang, J. Ma, H. Zhang, N. Shinya and L.-C. Qin, *Phys. Chem. Chem. Phys.*, 2011, **13**, 17615–17624.
14 Z. Niu, J. Chen, H. H. Hang, J. Ma and X. Chen, *Adv. Mater.*, 2102, **24**, 4144–4150.
15 Y. Zhang, L. Y. Zhang, P. Kim, M. Ge, Z. Li and C. W. Zhou, *Nano Lett.*, 2012, **12**, 2810–2816.
16 Z. P. Chen, W. C. Ren, L. B. Gao, B. L. Liu, S. F. Pei and H. M. Cheng, *Nat. Mater.*, 2011, **10**, 424–428.
17 Y. X. Xu, K. X. Sheng, C. Li and G. Q. Shi, *ACS Nano*, 2010, **4**, 4324–4330.
18 P. Guo, H. Song and X. Chen, *J. Mater. Chem.*, 2010, **20**, 4867–4874.
19 K. Sohn, Y. J. Na, H. Chang, K. Roh, H. D. Jang and J. Huang, *Chem. Commun.*, 2012, **48**, 5968–5970.
20 J. Hong, K. Char and B. Kim, *J. Phys. Chem. Lett.*, 2010, **1**, 3442–3445.
21 W. G. Leng, M. Chen, S. X. Zhou and L. Wu, *Langmuir*, 2010, **26**, 14271–14275.
22 J. P. Zhao, S. F. Pei, W. C. Ren, L. B. Gao and H. M. Cheng, *ACS Nano*, 2010, **4**, 5245–5252.
23 Z. Lei, N. Christova and X. S. Zhao, *Energy Environ. Sci.*, 2011, **4**, 1866–1873.
24 W. F. Chen and L. F. Yan, *Nanoscale*, 2011, **3**, 3132–3137.
25 J. Zhang, Y. Yu, L. Liu and Y. Wu, *Nanoscale*, 2013, **5**, 3052–3057.
26 Q. Du, M. Zheng, L. Zhang, Y. Wang, X. Wen, Y. Wang, J. Chen, L. Xue, W. Dai, G. Ji and J. Cao, *Electrochim. Acta*, 2010, **55**, 3897–3903.
27 W. Lv, D. Tang, Y. He, C. You, Z. Shi, X. Chen, C. Chen, P. Hou, C. Liu and Q. Yang, *ACS Nano*, 2009, **3**, 3730–3736.
28 Y. Qiu, X. Zhang and S. Yang, *Phys. Chem. Chem. Phys.*, 2011, **13**, 12554–12558.
29 D. Zhang, T. Yan, L. Shi, Z. Peng, X. Wen and J. Zhang, *J. Mater. Chem.*, 2012, **22**, 14696–14704.
30 M. Lee, C. Fan, Y. Wang, H. Li, J. Chang and C. Tsengd, *J. Mater. Chem. A*, 2013, **1**, 3395.
31 J. Qu, F. Gao, Q. Zhou and Z. Wang, *Nanoscale*, 2013, **5**, 2999–3005.